Quantum simulation of collinear $p+\mathrm{H}$ collisions in an intense laser field

Liang Feng[1] and Yu-kun Ho[2,1,*]
[1]*Institute of Modern Physics, Fudan University, Shanghai 200433, China*
[2]*CCAST (World Laboratory), P.O. Box 8730, Beijing 100080, China*
(Received 9 June 1999; published 10 January 2000)

The $p+\mathrm{H}$ collision in the presence of an intense laser field is studied by numerically solving the time-dependent one-dimensional Schrödinger equations. It is found that due to the enhanced ionization at the critical internuclear distance, the colliding particles can gain energy from the applied laser field. Also, the influences of the space distributions of the electronic and nuclear wave packets on the enhanced ionizations are discussed.

PACS number(s): 33.80.Rv, 33.80.Eh, 34.10.+x

I. INTRODUCTION

In recent years, much theoretical and experimental research has been devoted to the dissociative ionizations of molecules by intense laser fields [1–10]. Compared to the response of atoms to intense laser fields, the interactions of the molecules with intense laser fields are more complex, and the additional nuclear degrees of freedom result in some striking nonlinear phenomena. For example, it is found that the electron ionization rate is sensitive to the internuclear distance, and there is a so-called critical internuclear distance where the ionization rate reaches its maximum. Furthermore, in the presence of an intense laser field, the electrons in molecular ions can undergo either multiphoton excitations or ionizations by absorbing energy from the applied intense laser field. As a result, the two surface models, which are based on the Born-Oppenheimer separation of the nuclear and electronic degrees of freedom, cannot provide a good description of the competition between the dissociation and ionization. Thus, in some recent theoretical studies, the numerical solutions of the time-dependent Schrödinger equations are employed to investigate the mixed nuclear and electronic dynamics [6,7].

In our previous papers, an interesting mechanism concerning the gain of the nuclear kinetic energy during the $p+\mathrm{H}$ collisions in an intense laser field was explored by using the classical trajectory Monte Carlo (CTMC) simulations [11]. It is found that in these collisions, the intense laser fields induce strong correlations between the electronic and nuclear motions. On the one hand, the electron ionization rate depends on the internuclear distance. On the other hand, the enhanced electron ionization at the critical internuclear distance can result in an increase of the nuclear final kinetic energy. However, in the CTMC simulations, many important quantum effects, such as tunneling ionizations, are ignored. The main purpose of the present paper is just to give a detailed quantum description of $p+\mathrm{H}$ collisions in an intense laser field by numerically solving the one-dimensional (1D) time-dependent Schrödinger equations. Here, our emphasis is put on some basic features, such as the dependence of the ionization rate on the internuclear distance, and the corresponding nuclear kinetic-energy gain. Also, the influences of the space distribution of the electronic and nuclear wave packet on the enhanced ionizations are discussed.

In Sec. II a 1D model for collinear $p+\mathrm{H}$ collisions is briefly given. Here, a quantum wave function is employed to describe the electronic motion, while the proton is treated as a classical point particle. This approximation provides us a simple qualitative description of the dependence of the electronic dynamics on the internuclear distance, and hence, clearly shows the mechanism of the nuclear kinetic-energy gain. In Sec. III a full quantum description of this collisional process is presented. Here, we focus on the time evolution of the nuclear wave packet, and the effect of its space distribution on the enhanced ionization. Finally, Sec. IV contains a short summary.

*Corresponding address: Institute of Modern Physics, Fudan University, Shanghai 200433, People's Republic of China. FAX:+86-21-65104949. Electronic address: hoyk@fudan.ac.cn

II. THE KINETIC-ENERGY GAIN

In the present paper, we are mainly interested in some basic features of the atom-ion collisions in the presence of an intense laser field. So we will only consider collinear $p+\mathrm{H}$ collisions and make a further simplification that the electron and the two protons move just in one dimension along the electric field of the applied laser field. Namely, a 1D model is employed here. In fact, 1D models are frequently used to investigate the responses of molecules and atoms to intense laser fields, since they can provide useful qualitative descriptions while the difficulties with the numerical calculations are considerably reduced [7–10]. In addition, 1D models are also used to study various collisional processes [12,13].

In this section, the electron motion is described by a wave function $\phi(x,t)$, where x is the electron coordinate with respect to the center of mass of the two protons, and the two protons are treated directly by classical dynamics. Obviously, in the classical treatment, protons are considered as point particles and their space distributions are ignored. However, this approximation could give a clear description of the complex collisional processes, since important factors, such as the electron-tunneling ionization and the dependence of the electronic dynamics on the internuclear distance, are taken into account. Also, the influences of the nuclear space distribution will be discussed in Sec. III.

Thus, after separating the motion of the center of mass, one has (in a.u.)

$$i\frac{\partial\phi(x,t)}{\partial t}=[D_x+V(x,R(t))+qxE(t)]\phi(x,t), \tag{1a}$$

and

$$(m_p/2)\frac{d^2R(t)}{dt^2}=\frac{R(t)}{|R(t)|^3}+F(t), \tag{1b}$$

where

$$D_x=-\frac{1}{2\mu}\frac{\partial^2}{\partial x^2},$$

$$V(x,R(t))=\frac{-1}{[\{x-R(t)/2\}^2+1]^{1/2}}+\frac{-1}{[\{x+R(t)/2\}^2+1]^{1/2}}, \tag{1c}$$

$$\mu=\frac{2m_em_p}{m_e+2m_p},\quad q=1+m_e/(m_e+2m_p), \tag{1d}$$

and

$$F(t)=\int dx|\phi(x,t)|^2\left(\frac{-R(t)/2}{[\{x-R(t)/2\}^2+1]^{3/2}}+\frac{R(t)/2}{[\{x+R(t)/2\}^2+1]^{3/2}}\right). \tag{1e}$$

Here, $R(t)$ is the internuclear distance at time t, m_e and m_p are the electron and proton mass, respectively, and $E(t)$ is the applied laser electrical field. Note that in Eq. (1), the soft Coulomb potential is used to avoid the singularity of the Coulomb potential at $x=0$ [7]. In our calculations, $E(t)$ are assumed to be in the form of

$$E(t)=E_0U(t)\cos(\omega t), \tag{2a}$$

where E_0 is the amplitude of the laser electric field, and ω is the laser frequency. $U(t)$ denotes the envelope of the laser pulse that is given by

$$U(t)=\begin{cases} t/\tau_p, & 0<t<\tau_p \\ 1, & \tau_p<t<9\tau_p \\ (10\tau_p-t)/\tau_p, & 9\tau_p<t<10\tau_p \\ 0, & t>10\tau_p, \end{cases} \tag{2b}$$

where τ_p is the turn-on time of the laser pulse and is assumed to be 300 a.u. Equation 1(a) is numerically integrated by using the second-order split-operator method [7,14]. Thus, the electron wave function at time $t+\delta t$ is given by

$$\phi(x,t+\delta t)=\exp(-iD_x\delta t/2)\exp\{-i[V(x,R(t))+qxE(t)]\delta t\}\exp(-iD_x\delta t/2)\phi(x,t). \tag{3}$$

Meanwhile, the internuclear distance $R(t)$ is calculated by numerically integrating Eq. 1(b). The grid of the electron variable x is defined by the inequality $|x|<x_{\max}=70$ a.u. The spatial integration step is taken to be $\delta x=0.2$ a.u., and the time step δt is $\delta t=0.03$ a.u. To prevent the reflection of the wave function at the box edge, an absorbing mask function is introduced [6,7].

Also, it is assumed that at $t=0$, the initial internuclear distance is equal to 30 a.u. and the initial kinetic energy of the two protons is equal to 0.1 a.u. In addition, the electron in the target atom is assumed to lie in its ground state. The corresponding initial electron wave function is given by using the spectral method [14].

Figure 1 plots the time evolution of a typical $p+\mathrm{H}$ collision in a laser field with intensity 9×10^{13} W/cm^2 and wavelength 532 nm. Here, Figs. 1(a), 1(b), 1(c), and 1(d) display the internuclear separation $R(t)$, the electron ionization probability $P_I(t)$, the ionization rate $\alpha(t)$, and the kinetic energy of the protons $E_k(t)$ as functions of time, respectively. In our simulations, the electron outside a given region $|x|<d/2$ is considered to be ionized. Thus, the corresponding ionization probability $P_I(t)$ is calculated by

$$P_I(t)=1-\int_{-d/2}^{d/2}|\phi(x,t)|^2dx, \tag{4}$$

where the region width d is taken to be 70 a.u. The ionization rate $\alpha(t)$ is given by [6]

$$\alpha(t)=\frac{1}{\Delta t}\ln\left(\frac{1-P_I(t-\Delta t/2)}{1-P_I(t+\Delta t/2)}\right). \tag{5}$$

Here, the time interval Δt is chosen to be equal to $T/10$, where $T=2\pi/\omega$ is the cycle of the applied laser field. Also, it is noted that if a smaller time interval Δt is chosen, there is no significant change in our basic physical results, while some tiny peaks appear. Figure 1 clearly shows the dependence of the ionization rates on the internuclear distances. For example, in Fig. 1(c), there are two groups of the peaks of the ionization rate centered nearby at $t\sim1700$ a.u. and $t\sim2400$ a.u., respectively. Thus, from Figs. 1(a) and 1(c), it could be inferred that when the internuclear distance is within the range from 5 to 10 a.u., the ionization will be considerably enhanced. The enhanced ionizations are caused by the special structure of the combined potential generated by the applied laser fields and the two protons at the so-called critical internuclear separations. In Fig. 2, the combined potentials for three typical internuclear separations, i.e., $R=3$ a.u., $R=7$ a.u., and $R=15$ a.u., are schematically drawn. In each curve there are two potential wells centered at the target proton and the positive-charged projectile, respectively. At the beginning, the electron is bound in the left well generated by the target proton. When the internuclear separation is large (corresponding to the solid line in Fig. 2), although distorted by the applied laser field, the barrier of the atomic potential well is still too high for the electron to overcome, and thus, the atom will not be seriously ionized. But, when the projectile moves closer (the dashed line), the inner barrier between the two potential wells becomes lower, and thus, the electron is able to pass through the inner barrier and escape from the system directly. As a result, the ionization is greatly enhanced [8]. However, when the two protons get too close (the solid line with circles), the outer barrier becomes higher, which suppresses the ionization.

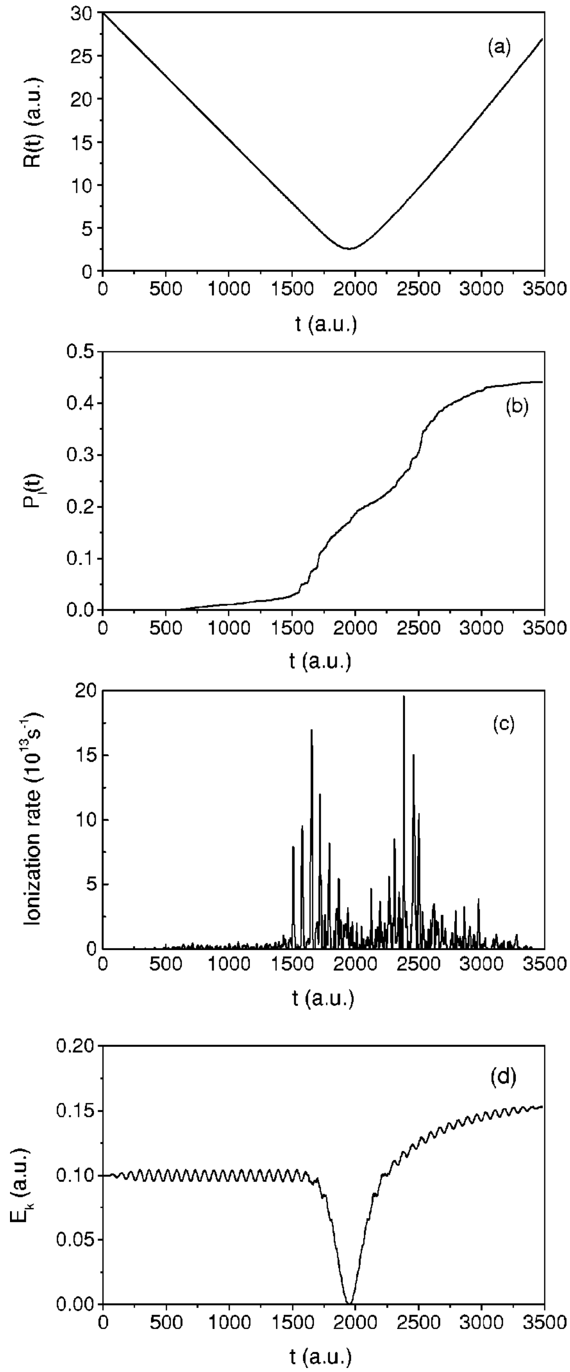

FIG. 1. The time evolution of a typical $p+\mathrm{H}$ collision in a laser field with intensity 9×10^{13} W/cm^2 and wavelength 532 nm. (a) The internuclear separation $R(t)$; (b) the ionization probability $P_I(t)$; (c) the ionization rate $\alpha(t)$; (d) the kinetic energy of the two protons $E_k(t)$.

Associated with the enhanced ionizations at the critical internuclear distance is an interesting gain of the nuclear kinetic energy shown in Fig. 1(d), where the nuclear kinetic energy is increased from its initial value 0.1 a.u. ($\sim$2.7 eV) to its final value 0.15 a.u. ($\sim$4.1 eV). This observation is just opposite to the scheme of the field-free $p+\mathrm{H}$ collisions, and furthermore, by this mechanism, nuclei can be heated by the applied intense laser fields [11]. Also, the dependence of the

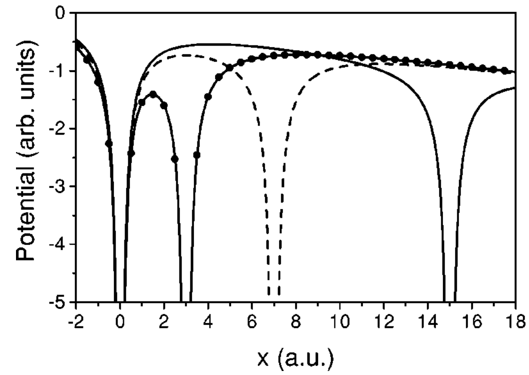

FIG. 2. The schematic of the combined potential generated by an intense laser field and two protons at three typical internuclear separations: $R=3$ a.u. (solid line with circles), $R=7.0$ a.u. (dashed line), and $R=15.0$ a.u. (solid line).

kinetic-energy gain, $\Delta E_k=E_k(t=3500)-E_k(t=0)$, on the laser intensity is investigated. We calculate the kinetic-energy gains for various laser intensities, and display the kinetic-energy gain ΔE_k as a function of laser intensities in Fig. 3, which shows that there is a noticeable kinetic-energy gain for the laser intensity range from $I=0.6\times10^{14}$ up to 1.6×10^{14} W/cm^2. Note that if the laser intensity is smaller than 1.3×10^{14} W/cm^2, ΔE_k increases with increasing laser intensity, and then decreases when the laser beam becomes stronger. This feature can be interpreted by the fact that the stronger laser will result in more ionizations, whereas too strong laser beams tend to cause serious ionization of the target atoms before the critical internuclear distance is reached, which would reduce the final kinetic-energy gain [11].

Now, we have a close observation of the enhanced ionization given in Fig. 1. In Figs. 4(a) and 4(b), the ionization rate $\alpha(t)$ and the laser electronic field $E(t)$ are plotted as functions of time, respectively. Note that at nearby $t\sim1700$ a.u., the ionization rate is quite small for the positive laser electric field, while sharp peaks occur when the laser electric field changes to negative. Here, the time interval between two neighboring peaks is about equal to the period of the laser field. However, after the collision ($t\sim2400$ a.u.), this simple regularity is broken down. To understand this striking feature, in Figs. 4(c) and 4(d), we present the space distributions of the electron probability density at two selected instants, i.e., $t=1550$ a.u. and $t=2450$ a.u. Here, the distribu-

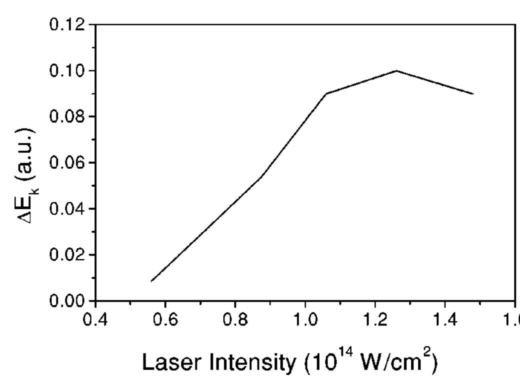

FIG. 3. The dependence of the kinetic-energy gain ΔE_k on the laser intensity I.

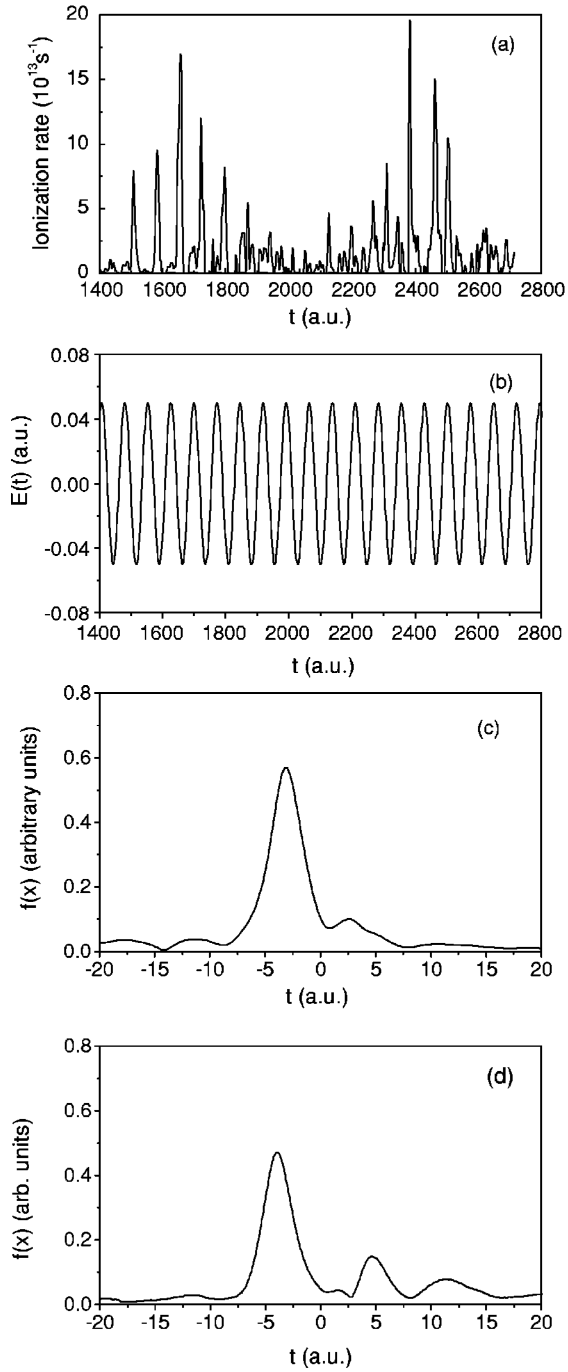

FIG. 4. The ionization feature associated with the asymmetrical distribution of the electron probability density. (a) The ionization rate vs time t. (b) The laser electric field $E(t)$ vs time t. (c) The electron probability density $f(x)$ at $t=1550$ a.u. (d) The electron probability density $f(x)$ at $t=2450$ a.u.

tion function $f(x)$ is calculated by

$$f(x)=|\phi(x,t)|^2.$$

Note that at $t=1550$ a.u. [see Fig. 4(c)], most of the electron probability distributes just around the left proton (i.e., the atomic nucleus), and the magnitude of $f(x)$ is quite small for $x>0$. In the above discussions, it has been pointed out that a sufficiently strong laser field can so significantly modify the Coulomb potential generated by the two protons at the critical internuclear distance that the electron is able to escape from the system by tunneling through the relatively small inner barrier between the two potential wells. Thus, when the electron moving around the left proton is driven by a negative laser electric field, it can pass through the inner barrier at its right side, and finally escape from the colliding system. However, when the applied laser electric field becomes positive, this enhanced ionization mechanism does not work for the electron at the left potential well. So, the high peaks of the ionization rates appear only when the laser electric field is negative. After the collision, the electron space distribution changes. For example, at $t=2450$ a.u. [see Fig. 4(d)], the distribution function $f(x)$ for $x>0$ is much higher than that at $t=1550$ a.u. In this case, the positive laser electric field can help the electron around the right proton pass through the inner barrier and escape from the system. Thus, for both the negative and positive laser electric fields, there are noticeable ionizations. Meanwhile, since more electrons distribute in the left potential well, the ionization rates are higher for the negative laser electronic field than those for the positive laser electronic field.

Also, Fig. 4 suggests that near critical internuclear distance, the electron cannot move freely between the two potential wells of the two protons, and tends to be trapped in one of them. As a result, the rate at which the electronic probability density disperses from one potential well to another is considerably slow, which implies that the slow nuclear motion might have a strong influence on the enhanced ionizations.

III. THE EVOLUTION OF THE NUCLEAR WAVE PACKET

Now, we begin to investigate the time evolution of the nuclear wave packet. Here, the system is described by the wave function $\psi(x,R,t)$, where x is the electron coordinate and R is the internuclear distance. In an intense laser field given by Eq. (2), the time evolution of the wave function is determined by

$$i\frac{\partial\psi(x,R,t)}{\partial t}=[D_x+V(x,R)+D_R+1/R+qxE(t)]\psi(x,R,t), \tag{6a}$$

where

$$D_R=-\frac{1}{m_p}\frac{\partial^2}{\partial R^2},$$

$$V(x,R)=\frac{-1}{[(x-R/2)^2+1]^{1/2}}+\frac{-1}{[(x+R/2)^2+1]^{1/2}}. \tag{6b}$$

Equation (6) is solved by using the two-dimensional split-operator method. Here, the grid of the electron variable x is just the same as that in Sec. II, while the grid of the internuclear distance R is defined by 0.35 a.u. $<R<$70 a.u. with

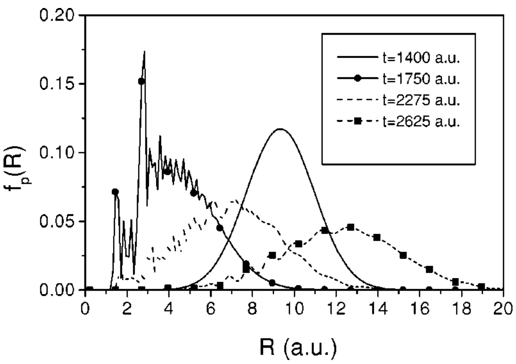

FIG. 5. The evolution of the nuclear distribution function $f_p(R)$.

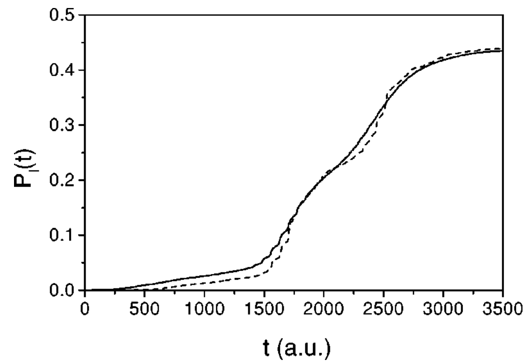

FIG. 6. The time evolution of the electron ionization probability $P_I(t)$. Here, the solid line is given by the full quantum calculation, while the dashed line corresponds to the simplification that the proton is treated as a classical point particle.

$\delta R=0.05$ a.u. The time step of the numerical integration is chosen to be $\delta t=0.03$ a.u. Since during the laser pulse, almost no nuclei can reach the boundary $R_{\max}=70$ a.u., no absorbing mask function at the nuclear boundary is introduced.

The initial wave function is assumed to be in the form of

$$\psi(x,R,t=0)=\phi_0(x)\chi(R), \tag{7}$$

where the initial electronic wave function $\phi_0(x)$ is just the same as that used in Sec. II, and the nuclear wave packet $\chi(R)$ is given by

$$\chi(R)=C\exp\{-(R-R_0)^2/2W_0^2-i\sqrt{m_pE_{k0}}R\}. \tag{8}$$

Here, C is the normalization constant, $R_0=30$ a.u. is the initial internuclear distance, $W_0=2.0$ a.u. is the initial width of the nuclear wave packet, and $E_{k0}=0.1$ a.u. is the initial nuclear kinetic energy.

For the laser pulse used in Sec. II, we calculate the time evolution of the wave function $\psi(x,R,t)$, and in Fig. 5, the corresponding nuclear space distributions for four typical instants are displayed. Here, the nuclear distribution function $f_p(R)$ is calculated by

$$f_p(R)=\int dx|\psi(x,R,t)|^2. \tag{9}$$

In Fig. 5, one sees that, when the averaged internuclear distance is quite large (corresponding to the solid line), the nuclear distribution function $f_p(R)$ is in the form of the Gaussian wave packet. At $t=1750$ a.u. (the solid line with circles), the averaged internuclear distance is reduced to about 4.0 a.u., and hence, the two protons experience a strong repulsive Coulomb potential. As a result, the front part of the incident nuclear wave packet is reflected, while the other is still coming. So, $f_p(R)$ oscillates quickly. At $t=2275$ a.u. (the dashed line), the nuclear distribution function $f_p(R)$ becomes a Gaussian wave packet again, and its center is pushed to 7 a.u. by the repulsive Coulomb potential. Finally, at $t=2625$ a.u. (the dashed line with squares), the center of the nuclear wave packet moves to 12 a.u.

To show the influence of the space distributions of the nuclear wave packets on the enhanced electron ionizations, in Fig. 6, we compare the ionization probability calculated by the full quantum treatment with that given in Sec. II. Here, the solid curve is given by the full quantum calculations, and the dashed one represents the result of the classical treatment of the nuclear motion. Qualitatively, the two curves agree with each other quite well. However, in the dashed curve, there are two separate rapid increases at $t\sim1600$ and $t\sim2300$ a.u., respectively, whereas in the solid line, the ionization probability increases with almost the same rates in the time range from $t=1600$ to $t=2700$ a.u. Partly, this difference comes from the fact that in the full quantum treatment, the proton distributes in a broad space range instead of a point, which means that the enhanced ionizations could be observed for a wider time range.

IV. CONCLUSIONS

In conclusion, based on an 1D quantum model, we have studied $p+\mathrm{H}$ collisions in the presence of an intense laser field. It is found that the electron ionization rate will be considerably enhanced at the critical internuclear distance. Also, the enhanced ionizations can result in an increase of the kinetic energy of the protons. This energy absorption mechanism is of practical interest, since by it, the energy of the applied laser pulse can be directly transferred to the nuclei. In addition, some features of the $p+\mathrm{H}$ collisions in the presence of an intense laser field are investigated. Especially, the influences of the space distributions of the electronic and nuclear wave packets on the enhanced ionizations are discussed.

However, there are many questions left open for future studies. For example, due to the introduction of an absorbing mask function at the electron boundary, the full quantum calculations in the present paper are not able to provide the correct energy spectrum of the colliding protons. We plan to discuss these problems in other places.

ACKNOWLEDGMENTS

This work was partly supported by Project No. 19804002 of the National Science Foundation of China, National High-Tech ICP Committee in China, the Youth Science Foundation of the Shanghai Education Department, and the Science Foundation of Fudan University.

[1] C. Cornaggia, D. Normand, and J. Morellec, J. Phys. B **25**, L415 (1992).
[2] D. Normand and M. Schmidt, Phys. Rev. A **53**, R1958 (1996).
[3] P. A. Hatherly, M. Stankiewicz, K. Codling, L. J. Frasinski, and G. M. Cross, J. Phys. B **27**, 2993 (1994).
[4] E. Constant, H. Stapelfeldt, and P. B. Corkum, Phys. Rev. Lett. **76**, 4140 (1996).
[5] K. C. Kulander, F. H. Mies, and K. J. Schafer, Phys. Rev. A **53**, 2562 (1996).
[6] S. Chelkowski, A. Conjusteau, T. Zuo, and A. D. Bandrauk, Phys. Rev. A **54**, 3235 (1996).
[7] J. Ludwig, H. Rottke, and W. Sandner, Phys. Rev. A **56**, 2168 (1997).
[8] D. M. Villeneuve, M. Yu. Ivanov, and P. B. Corkum, Phys. Rev. A **54**, 736 (1996).
[9] H. Yu and A. D. Bandrauk, Phys. Rev. A **56**, 685 (1997).
[10] S. Chelkowski, C. Foisy, and A. D. Bandrauk, Phys. Rev. A **57**, 1176 (1998).
[11] L. Feng and Yu-kun Ho, Phys. Rev. A **58**, 2332 (1998); Phys. Lett. A **251**, 121 (1999).
[12] R. Kosloff, J. Chem. Phys. **79**, 1823 (1983).
[13] D. E. Fitz and Paul Brumer, J. Chem. Phys. **70**, 5527 (1979).
[14] Mark R. Hermann and J. A. Fleck, Jr., Phys. Rev. A **38**, 6000 (1988).